Chinese Chemical Letters 34 (2023) 107941

Contents lists available at ScienceDirect

Chinese Chemical Letters

journal homepage: www.elsevier.com/locate/cclet

Bubble transfer on wettability-heterogeneous surfaces

Chunhui Zhang[a,b,c], Xiao Xiao[d], Ziwei Guo[c], Lei Jiang[a], Cunming Yu[c,*]

[a] CAS Key Laboratory of Bio-inspired Materials and Interfacial Science, Technical Institute of Physics and Chemistry, Beijing 100190, China
[b] School of Chemical Sciences, University of Chinese Academy of Sciences, Beijing 100049, China
[c] Key Laboratory of Bio-inspired Smart Interfacial Science and Technology of Ministry of Education, School of Chemistry, Beihang University, Beijing 100191, China
[d] Department of Electrical and Computer Engineering, National University of Singapore, Singapore 117583, Singapore

ARTICLE INFO

Article history:
Received 4 October 2022
Revised 19 October 2022
Accepted 24 October 2022
Available online 23 May 2023

Keywords:
Bubble transfer
Superaerophilicity
Wettability-heterogenous
Surface energy
Bubble collection
Water splitting

ABSTRACT

Researches have investigated the formation, transportation and spreading of bubble on solid surface with specific wettability. However, bubble transfer on wettability-heterogeneous surfaces has been rarely reported, which also plays significant role in water electrolysis, heat transfer, micro-bubble collection, *etc.* In this work, we carefully investigate the behavior of bubble transfer from the aerophobic or aerophilic region to the superaerophilic region through fabricating the wettability-heterogenous surfaces. Surface energy was elucidated to be transformed to the kinetic energy during bubble transfer process. Theoretical analysis on the average velocity of bubble transfer was consistent with the experimental results. The influence of wettability of solid substrate, bubble volume and superaerophilic stripe width on bubble transfer are carefully investigated. Moreover, wettability-heterogeneous surfaces were explored to be applied in micro-CO_2 bubble collection and H_2 bubble removement in water splitting.

Bubble behaviors in aqueous medium play a critical role in both biological and industrial processes, such as plastron respiration [1–3], drag reduction [4–6], heat transfer [7–9], and gas-involved reaction [10–13]. However, gas bubbles in liquid system could cause serious problems. Examples include the cavitation erosion in high-velocity flow, which would reduce lifetime of underwater equipment [14–16], and serious bubble adhesion on gas evolution electrode, which would block catalytic sites and thus result inefficient electrode reaction [17–19]. Hence, deeply understanding bubble properties on solid surface and regulating bubble behaviors with a controllable manner in aqueous system are urgently needed in both scientific research and industrial applications.

In 2009, Wang *et al.* firstly reported that the air bubble can quickly burst within several milliseconds on superhydrophobic lotus leaf [20]. Since then, wettability/superwettability of gas bubbles has been proposed and developed, which could be regarded as the complementary process of liquid wettability on the solid surface [21–23]. Superhydrophobic lotus leaf immersed in water is a classic example of superaerophilic interface. Meanwhile, controllable bubble manipulations based on gas-wettability have been widely invented [24–26]. For example, gas bubbles tend to adhere and spread on superhydrophobic/superaerophilic materials, which have been proved as promising materials for bubble delivery and collection [27–29]. On the contrary, superhydrophilic materials, which is superaerophobic in aqueous solution, show extremely low adhesive force and can be applied to promote bubble detachment [30,31]. Owing to large adhesive to gas bubble and low motion resistance, slippery materials also show the potential capability in bubble manipulations [32–35]. Current researches have mainly focused on understanding spreading and delivery of bubble at surface with one specific wettability. For example, Quéré *et al.* carefully discussed the dynamic of complete spreading of bubble on superaerophilic solid surface [36]. Megaridis *et al.* investigated later spreading of gas bubbles on wettability-confined superaerophilic track [37]. Droplet motions on wettability-heterogeneous surface have been investigated and applied in ice-removing and water condensation [38,39]. However, bubble behaviors on wettability-heterogeneous surface, which is also important in heterogeneous interfacial process, have been rarely investigated.

In this contribution, we carefully investigated the bubble transfer process on wettability-heterogeneous surface, *i.e.*, the aerophilic/superaerophilic surface and the aerophobic/superaerophilic surface, through fabricating the superaerophilic (SAL) stripe on the aerophilic or the aerophobic solid substrate. The bubble, initially locating at aerophilic or aerophobic substrate region, will be immediately transferred to SAL stripe in several milliseconds when contacts with the edge of the SAL stripe. The

* Corresponding author.
E-mail address: ycmbhs@iccas.ac.cn (C. Yu).

https://doi.org/10.1016/j.cclet.2022.107941
1001-8417/

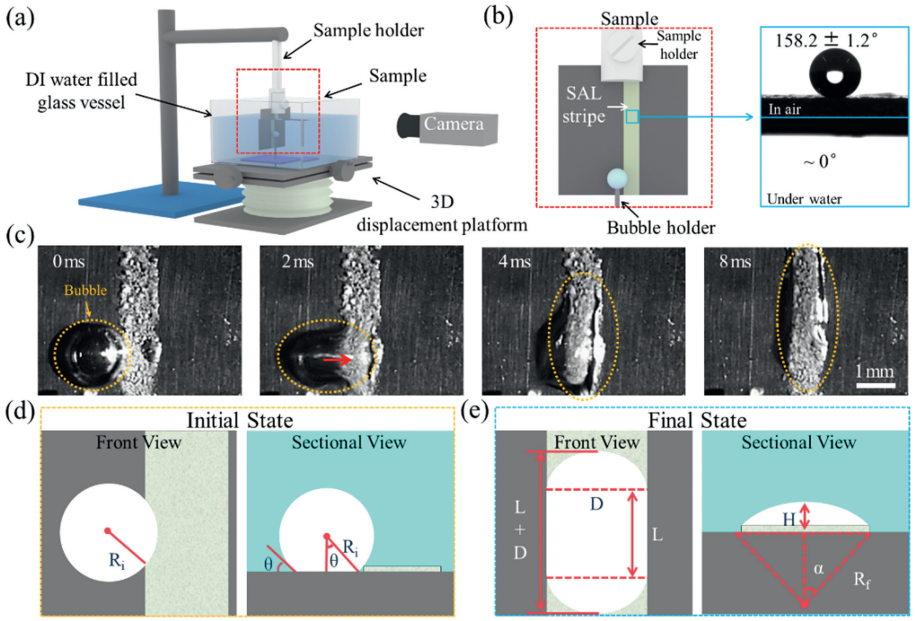

Fig. 1. (a) Schematic diagram of experimental setup for bubble transfer imaging. (b) Schematic diagram of solid substrate coated with superaerophilic (SAL) stripe, the SAL stripe shows superaerophobicity in air and superaerophilicity under water. (c) Optical images of bubble transfer from solid substrate to SAL stripe. Schematic diagram of bubble morphology (d) before and (e) after bubble transfer process.

wettability of substrate, bubble volume and SAL stripe width have great influence on bubble transfer velocity. Typically, substrate with larger bubble contact angle (BCA), bubble with smaller volume and SAL stripe with larger width, are favorable for faster bubble transfer. From point-view of surface energy, we theoretically calculated bubble transfer velocity, which is consistent with experimental results. Benefited from fast bubble transfer on wettability-heterogeneous surface, efficient CO_2 bubble collection in soda water and timely H_2 bubble removement in water splitting are successfully achieved, showing potential application in real-world.

The bubble transfer process was investigated *via* a micro-bubble imaging system (Fig. 1a). Prepared sample was fixed through a sample holder and immersed in deionized (DI) water filled glass vessel. A bubble holder was placed in vessel bottom and bubble with specific volume was introduced on bubble holder through a micro-syringe. Bubble position can be precisely controlled through a 3D displacement platform. A high-speed camera was placed in front of sample and could clearly observe and record the bubble behaviors. The wettability-heterogeneous sample was prepared through the successive processes of mask attachment, SAL modification and mask removement (Fig. S1 in Supporting information). Finally, the sample composed of solid substrate and SAL stripe can be successfully prepared (Fig. 1b). The SAL stripe shows superhydrophobicity in air with water contact angle of ~158.2°, and superaerophilicity underwater with BCA of ~0° (insets in Fig. 1b), which is attributed to numerous superaerophilic nanoparticles on SAL stripes (Fig. S2 in Supporting information). As shown in Fig. 1c and Movie S1 (Supporting information), a gas bubble was firstly introduced and adhered on solid substrate region. When contact SAL stripe, the bubble immediately transferred from solid substrate to SAL stripe in several millisecond, showing fast bubble transfer ability. The fast bubble transfer velocity is proposed to be originated from the released surface energy of the whole transfer system. For a given system, the total surface energy E can be expressed as follows [40]:

$$E = A\gamma_{water,vapor} + B\gamma_{water,solid} + C\gamma_{solid,vapor} \quad (1)$$

where A, B, C are surface area of water/vapor, water/solid, solid/vapor interfaces, respectively. $\gamma_{\text{water, vapor}}$, $\gamma_{\text{water, solid}}$, $\gamma_{\text{solid, vapor}}$ are corresponding interface tensions.

The initial bubble morphology before bubble transfer can be assumed as a spherical cap (Fig. 1d), of which radius R_i can be calculated with follow equation:

$$R_i = \left(\frac{3V}{2\pi\left(1 + \frac{3}{2}\cos\theta - \frac{\cos^3\theta}{2}\right)} \right)^{\frac{1}{3}} \quad (2)$$

where θ is supplementary angle of BCA, V is the bubble volume. Assume surface area of solid substrate and SAL stripe are M, N respectively and the SAL stripe is covered by a thin layer gas cushion, of which surface area is same as SAL stripe, then:

$$A_i = s_{\text{shperical cap}} + s_{\text{gas cushion}} = 2\pi R_i^2(1 + \cos\theta) + N \quad (3)$$

$$C_i = \pi (R_i \sin\theta)^2 \quad (4)$$

$$B_i = M - C_i = M - \pi (R_i \sin\theta)^2 \quad (5)$$

At final state, bubble transferred from solid substrate to SAL stripe and merging into gas cushion existed on SAL stripe. Transported bubble morphology can be assumed as sum of spherical cap and partial cylinder. Typical geometry factors D, H, L, R_f, α are presented in Fig. 1e and satisfy the following equations:

$$V = \frac{\pi H\left(3D^2 + 4H^2\right)}{24} + \left(\alpha R_f^2 - \frac{D\left(R_f - H\right)}{2}\right)L \quad (6)$$

$$\tan\frac{\alpha}{2} = \frac{2H}{D} \quad (7)$$

$$R_f \cos\alpha + H = R_f \quad (8)$$

where D is width of SAL stripe, V is bubble volume, L is bubble length after horizontal transfer which can be measured through

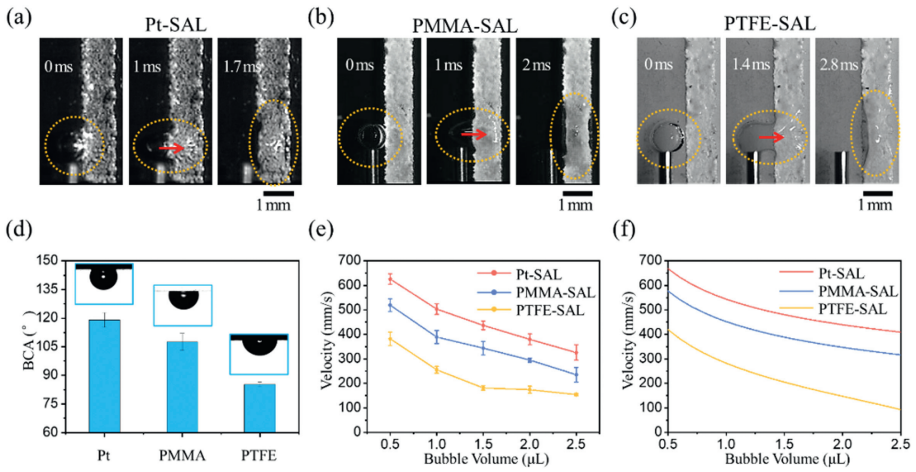

Fig. 2. Optical images of bubble transfer on (a) Pt-SAL, (b) PMMA-SAL, (c) PTFE-SAL surface. (d) BCAs of various solid substrate, insets showed corresponding bubble contact state. (e) Experimentally measured and (f) theoretically calculated bubble transfer velocity as a function of bubble volume at given wettability-heterogeneous surface.

optical image. Numerically solve Eqs. 6-8, R_f, α and H can be obtained. Then A_f, B_f, C_f can be calculated as follows:

$$A_f = \left(N - \pi \cdot \frac{D^2}{4} - D \cdot L\right) + 2\pi R_f H + 2\alpha R_f L \tag{9}$$

$$B_f = M \tag{10}$$

$$C_f = 0 \tag{11}$$

Difference of surface energy between final state and initial state can be expressed as follows:

$$\Delta E = E_f - E_i = \left(A_f - A_i\right)\gamma_{\text{water,vapor}} + \left(B_f - B_i\right)\gamma_{\text{water,solid}} + \left(C_f - C_i\right)\gamma_{\text{solid,vapor}} \tag{12}$$

The assumed M, N go away during the calculation of Eq. 12, and the value of ΔE can be exactly obtained. The resistance force (F_D) of water to hinder bubble movement during bubble transfer process can be expressed as follows [41]:

$$F_D = \frac{1}{2} C_D \rho_w v^2 A_{cs} \tag{13}$$

where C_D is the drag coefficient of water, ρ_w is the density of water, A_{cs} is the cross-sectional area of gas bubble and can be estimated as average sectional area of initial state and final state:

$$A_{cs} = \frac{1}{2}\left\{\left[(\pi - \theta)R_i^2 + \frac{1}{2}R_i^2 \sin(2\theta)\right] + \left[\alpha R_f^2 - \frac{1}{2}R_f^2 \sin(2\alpha) + L \cdot H\right]\right\} \tag{14}$$

During bubble transfer process, the surface energy is converted to bubble kinetic energy. Considering the work done by F_D and assuming a constant velocity transfer, the energy conservation formula during bubble transfer process can be illustrated as follows:

$$\frac{1}{2}(\rho_w + \rho_b)V v^2 + F_D.d = -\Delta E \tag{15}$$

where ρ_b is the density of bubble, which can be regarded as zero. v is average transfer velocity of gas bubble; d is bubble transfer distance and can be estimated as $(R_i \sin\theta + 0.5D)$. Then the transfer velocity can be theoretically calculated.

Wettability of solid substrate, which is related to $\gamma_{\text{water,solid}}$ and $\gamma_{\text{solid,vapor}}$ in Eq. 12, has great influence on bubble transfer velocity. To eliminate the interference of roughness, smooth platinum (Pt), polymethylmethacrylate (PMMA), and polytetrafluoroethylene (PTFE) sheets were chosen as the solid substrate (Fig. S3 in Supporting information). As shown in Figs. 2a-c, bubble transferred from Pt, PMMA, PTFE surface to SAL stripe in 1.7 ms, 2.0 ms and 2.8 ms, respectively, showing increased transfer time. Comsol simulation results in Fig. S4 showed that bubble transfer times on Pt-SAL, PMMA-SAL, PTFE-SAL surface are increased from 2.4 ms to 3.0 ms, which is consistent with the tendency presented in Figs. 2a-c. The BCAs of Pt, PMMA, PTFE are $119.1° \pm 3.9°$, $107.5° \pm 4.4°$, $85.2° \pm 1.3°$, respectively (Fig. 2d), which is attributed to decreased solid/vapor interface energy and will lower bubble transfer velocity. The related interface tensions of Pt, PMMA and PTFE substrate are presented in Table S1 (Supporting information) [42,43]. Both the experimental results (Fig. 2e) and theoretically calculated results from the point view of surface energy (Fig. 2f) verified this propose. For example, experimentally measured 1.5 μL bubble transfer velocities from Pt, PMMA, PTFE to 1 mm wide SAL stripe are 437.0 ± 17.2 mm/s, 344.0 ± 27.1 mm/s, 181.7 ± 9.1 mm/s, respectively. While theoretically calculated results are 481 mm/s, 388 mm/s, 205 mm/s, respectively. Note, theoretically calculated velocity is a little higher than measured velocity, which may be caused by simplified assumption of bubble morphology and approximate treatment of resistance. From Figs. 2e and f, we also learned that smaller bubble volume is favorable for faster transfer velocity at a given wettability-heterogeneous surface.

These phenomena can also be explained through the point-view of Laplace pressure. As shown in Fig. S5 and Note S1 (Supporting information), the Laplace pressure difference between bubble on solid substrate and gas cushion on SAL stripe can be expressed as follows:

$$\Delta p = \frac{2\gamma}{R_{\text{bubble}}} - \frac{\gamma}{\frac{H}{2} + \frac{D^2}{8H}} \tag{16}$$

where γ is surface tension of water, H is the thickness of gas cushion, D is the width of SAL stripe. For bubbles with a given volume, relatively larger BCA on solid substrate will result in smaller R_{bubble}, which consequently lead to larger Laplace pressure difference Δp and promote faster bubble transfer. For a given wettability-heterogeneous surface, increasing bubble volume will reduce Δp, and thus result lower bubble transfer velocity.

SAL stripe width also has great influence on bubble transfer. As shown in Figs. 3a-c, 1.5 μL bubble transfer time on Pt-SAL surface with SAL width of 0.75 mm, 1.00 mm and 1.50 mm are 3.6 ms, 2.8 ms and 2.5 ms, respectively, showing decreased transfer time. Fig. 3d presented the experimental bubble transfer velocity as a function of bubble volume on Pt-SAL surface

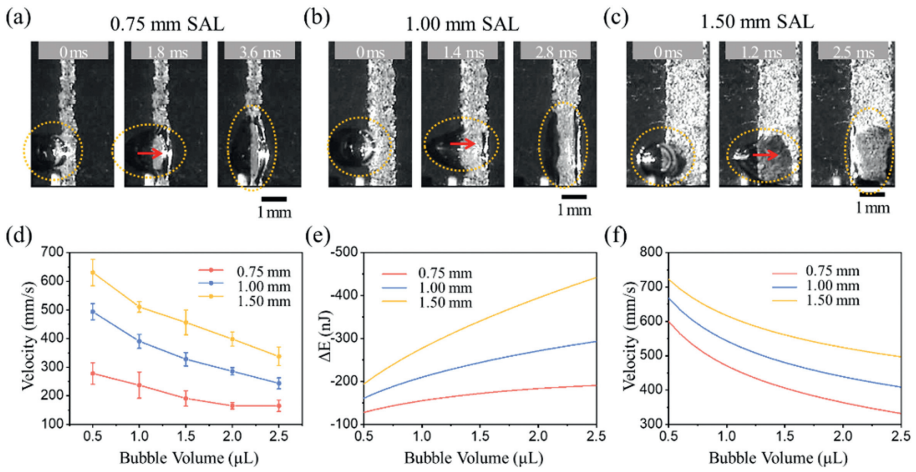

Fig. 3. Optical images of bubble transfer on Pt-SAL surface with SAL width of (a) 0.75 mm, (b) 1.00 mm, (c) 1.50 mm. (d) Experimentally measured bubble transfer velocity as a function of bubble volume on Pt-SAL surface with specific SAL width. (e) Theoretically calculated surface energy change and (f) bubble transfer velocity as a function of bubble volume at Pt-SAL surface with specific SAL width.

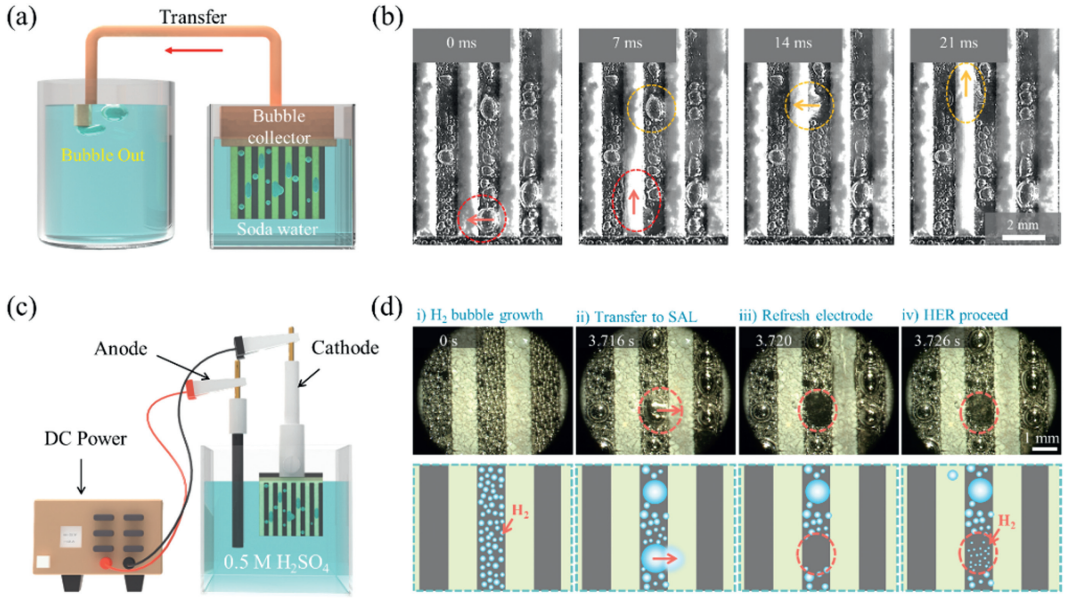

Fig. 4. (a) Schematic diagram of experimental setup for bubble collection. Pt substrate with SAL stripes (Pt-SALs) was immersed into soda water to collect CO_2 bubbles. (b) *In-situ* observations of bubble transfer process. The generated CO_2 bubbles on Pt substrate can be transferred through SAL stripes. (c) Schematic diagram of experimental setup for water splitting. Pt-SALs were set as cathode to produce H_2 bubbles. (d) *In-situ* observations of bubble generation and transfer on Pt-SALs electrode.

with various SAL stripe width. At a given bubble volume, the bubble transfer velocity is increased with the enlarging of SAL stripe width. For instance, when SAL stripe widths are 0.75 mm, 1.00 mm, 1.50 mm, the 1.5 μL bubble transfer velocities are 190.5 ± 26.3 mm/s, 327.8 ± 23.4 mm/s, 456.2 ± 43.2 mm/s, respectively. Increasing bubble volume, the bubble transfer velocities gradually decreased. For example, when bubble volumes are 0.5 μL, 1.0 μL, 1.5 μL, 2.0 μL, 2.5 μL, the bubble transfer velocities from Pt to 0.75 mm SAL stripe are 493.4 ± 28.0 mm/s, 390.2 ± 24.3 mm/s, 327.8 ± 23.4 mm/s, 285.4 ± 13.4 mm/s, 243.5 ± 19.0 mm/s, respectively. The difference of surface energy during bubble transfer is theoretically calculated and presented in Fig. 3e. For bubble with same volume, larger SAL stripe width will result larger surface energy change. At a given SAL stripe width, the surface energy change is gradually increased with bubble volume. Considering resistance of water and energy conversion formula (Eq. 15), average bubble transfer velocity can be successfully obtained (Fig. 3f), which is consistent with the velocity change trend of experimental results in Fig. 3d. Also, learned from Eq. 16, large SAL stripe width D can increase Laplace pressure difference Δp and promote bubble transfer.

Microbubbles in aqueous solution could cause serious corrosion of underwater metal equipment because of its long residence time in water [44,45]. Owing to best bubble transfer performance, the Pt-SALs surface was applied to collect and remove micro-bubbles in aqueous solution. Experimental setup is presented in Fig. 4a. Soda water, as an efficient solution to generate CO_2 microbubbles, was selected as test solution. The prepared sample was immersed in soda water to test the bubble collection ability. As shown in Fig. S6 and Movie S2 (Supporting information), numerous tiny bubbles generated and were transferred to bubble collector and then be released in another vessel *via* a plastic tube, which shows the ability of collecting and removing microbubbles in aqueous solution. Fig. 4b shows detailed observations of bubble transfer on wettability-heterogeneous surface in soda water. Micro bubble firstly generated at solid substrate. With growing up, bubble contacts the SAL

stripe and can be immediately transferred. Single bubble transfer process takes only several milliseconds, which shows great potential applications in micro-bubble removing and collection. Besides, this design can also be applied in water splitting to timely remove adhered bubbles on hydrogen evolution electrode (Fig. 4c). As shown in Fig. 4d and Movie S3 (Supporting information), prepared Pt-SALs was immersed in 0.5 mol/L H_2SO_4 and applied with negative potential of −2 V to produce H_2: (i) H_2 bubbles generated at Pt region and coalesced with adjacent bubble into bigger bubble. (ii) With bubble grew up, the adhered H_2 bubble contact with SAL stripe and be transferred immediately. (iii) After bubble transfer, fresh electrode surface exposed and (iv) hydrogen evolution proceeded. The fast bubble transfer ability on Pt-SALs electrode endows the electrode with enough fresh surface to continuously produce hydrogen.

In conclusion, both experimental and theoretical investigation of bubble transfer behaviors on wettability-heterogeneous surface were carefully discussed. Bubble on aerophobic substrate, *i.e.*, Pt and PMMA, or aerophilic substrate, *i.e.*, PTFE, can be transferred to SAL stripes in several milliseconds, which can be attributed to surface energy change during bubble transfer. Wettability of substrate, bubble volume and SAL stripe width have great influence on bubble transfer velocity. The study provides a theoretical model to predict bubble behaviors on wettability-heterogeneous surface and supplies potential applications of wettability-heterogeneous surface in real world, including micro-bubbles collection and water splitting.

Declaration of competing interest

The authors declare that they have no known competing financial interests or personal relationships that could have appeared to influence the work reported in this paper.

Acknowledgments

The authors gratefully acknowledge the National Natural Science Foundation (Nos. 22175011, 22005015)

Supplementary materials

Supplementary material associated with this article can be found, in the online version, at doi:10.1016/j.cclet.2022.107941.

References

[1] M.R. Flynn, J.W.M. Bush, J. Fluid Mech. 608 (2008) 275–296.
[2] S. Kehl, K. Dettner, J. Morphol. 270 (2009) 1348–1355.
[3] R.S. Seymour, S.K. Hetz, J. Exp. Biol. 214 (2011) 2175–2181.
[4] C. Yu, M. Liu, C. Zhang, et al., Giant 2 (2020) 100017.
[5] D. Saranadhi, D.Y. Chen, J.A. Kleingartner, et al., Sci. Adv. 2 (2016) 9.
[6] K. Fukagata, N. Kasagi, P. Koumoutsakos, Phys. Fluids 18 (2006) 4.
[7] L. Zhang, H.Z. Liu, X.J. Liu, D.Q. Chen, Int. J. Heat Mass Transf. 196 (2022).
[8] J. Zou, H. Zhang, Z. Guo, et al., Langmuir 34 (2018) 14096–14101.
[9] R.F. Wen, Q. Li, W. Wang, et al., Nano Energy 38 (2017) 59–65.
[10] J. Cao, J. Zhou, M. Li, et al., Chin. Chem. Lett. 33 (2022) 3745–3751.
[11] Y.L. Yang, Y. Tang, H.M. Jiang, et al., Chin. Chem. Lett. 30 (2019) 2089–2109.
[12] Y.X. Wang, F.T. He, L. Chen, et al., Chin. Chem. Lett. 31 (2020) 2668–2672.
[13] Y.M. Liu, H.L. Yang, X.F. Fan, B. Shan, T.J. Meyer, Chin. Chem. Lett. 33 (2022) 4691–4694.
[14] C.A. Fairfield, Wear 317 (2014) 92–103.
[15] A. Philipp, W. Lauterborn, J. Fluid Mech. 361 (1998) 75–116.
[16] S. Fontanesi, M. Giacopini, G. Cicalese, S. Sissa, S. Fantoni, Eng. Fail. Anal. 44 (2014) 408–423.
[17] J. Dukovic, C.W. Tobias, J. Electrochem. Soc. 134 (1987) 331–343.
[18] J. Eigeldinger, H. Vogt, Electrochim. Acta 45 (2000) 4449–4456.
[19] C. Gabrielli, F. Huet, R.P. Nogueira, Electrochim. Acta 50 (2005) 3726–3736.
[20] J. Wang, Y. Zheng, F. Nie, J. Zhai, L. Jiang, Langmuir 25 (2009) 14129–14134.
[21] C. Yu, P. Zhang, J. Wang, L. Jiang, Adv. Mater. 29 (2017) 1703053.
[22] P. Zhang, S. Wang, S. Wang, L. Jiang, Small 11 (2015) 1939–1946.
[23] M. Liu, S. Wang, L. Jiang, Nat. Rev. Mater. 2 (2017) 17036.
[24] J. Song, Z. Liu, X. Wang, et al., J. Mater. Chem. A 7 (2019) 13567–13576.
[25] H. Ma, M. Cao, C. Zhang, et al., Adv. Funct. Mater. (2017) 1705091.
[26] C. Yu, X. Zhu, M. Cao, et al., J. Mater. Chem. A 4 (2016) 16865–16870.
[27] C. Yu, M. Cao, Z. Dong, et al., Adv. Funct. Mater. 26 (2016) 6830–6835.
[28] R. Ma, J. Wang, Z. Yang, et al., Adv. Mater. 27 (2015) 2384.
[29] X. Chen, Y. Wu, B. Su, et al., Adv. Mater. 24 (2012) 5884–5889.
[30] M. Jiang, H. Wang, Y. Li, et al., Small 13 (2017) 1602240.
[31] Z. Lu, M. Sun, T. Xu, et al., Adv. Mater. 27 (2015) 2361–2366.
[32] C. Zhang, X. Xiao, Y. Zhang, et al., ACS Nano 16 (2022) 9348–9358.
[33] C. Zhang, B. Zhang, H. Ma, et al., ACS Nano 12 (2018) 2048–2055.
[34] Y. Jiao, X. Lv, Y. Zhang, et al., Nanoscale 11 (2019) 1370–1378.
[35] X. Tang, H. Xiong, T. Kong, et al., ACS Appl. Mater. Interfaces 10 (2018) 3029–3038.
[36] H. de Maleprade, C. Clanet, D. Quere, Phys. Rev. Lett. 117 (2016) 094501.
[37] M. Jafari Gukeh, T. Roy, U. Sen, R. Ganguly, C.M. Megaridis, Langmuir 36 (2020) 11829–11835.
[38] Y. Gurumukhi, S. Chavan, S. Sett, et al., Matter 3 (2020) 1178–1195.
[39] C.W. Lo, Y.C. Chu, M.H. Yen, M.C. Lu, Joule 3 (2019) 2806–2823.
[40] B.E. Pinchasik, J. Steinkühler, P. Wuytens, et al., Langmuir 31 (2015) 13734–13742.
[41] C. Yu, M. Cao, Z. Dong, et al., Adv. Funct. Mater. 26 (2016) 3236–3243.
[42] V. Leon, A. Tusa, Y.C. Araujo, Colloid Surface A 155 (1999) 131–136.
[43] A. Zdziennicka, A. Zdziennicka, B. Janczuk, B. Janczuk, Int. J. Adhes. Adhes. 84 (2018) 275–282.
[44] D.A. Lopez, T. Perez, S.N. Simison, Mater. Des. 24 (2003) 561–575.
[45] Z. Liu, X. Gao, L. Du, et al., Appl. Surf. Sci. 351 (2015) 610–623.